The Nature of Field Emission From Microparticles and the Ensuing Voltage Breakdown

Hasan Padamsee and Jens Knobloch

Floyd R. Newman Laboratory of Nuclear Studies, Cornell University, Ithaca, NY 14853

Abstract. In recent years there has been much progress in furthering our understanding of the sources of field emission as well as in tracing the stages from field emission to voltage breakdown. These advances come from microscopic studies (scanning electron microscopy, energy dispersive x-ray analysis, Auger spectroscopy) of field emitters located by DC high voltage scans as well as from field emitters found in microwave cavities. Craters, residues and starbursts found at breakdown sites reveal much about the physics of voltage breakdown. Both experiments and computer simulations show the important role played by gases generated by field emission induced heating.

I THE PHYSICS OF FIELD EMISSION

For background material on field emission and voltage breakdown there are several review articles in Refs. [1–6]. Recent books cover a wide range of topics [7, 8].

Very briefly, Fowler and Nordheim (FN) [9] showed that, in the presence of an electric field, electrons tunnel out of the metal into the vacuum because of their quantum wave-like nature. However, comparison between calculated and observed currents reveals that emission at a given field is substantially higher than the FN predictions. Traditionally, the excess has been attributed to a field enhancement factor β_{FN} arising from *hypothetical asperities* on the surface that supposedly enhance the electric field. Associated with these hypothetical asperities there is also the traditional emissive area, A_{e}.

Substantial advances in understanding the nature of field emission have been made by DC high-voltage studies that locate emission sites with a needle-shaped electrode, followed by electron microscopy of the sites. Much information about the nature of emitters has also come from superconducting RF (SRF) cavity experiments equipped with temperature-mapping capabilities. In an SRF cavity, the pattern of temperature rise as a function of position along a given meridian contains implicit information about the location and characteristics of the emission source. We can relate such symptoms to the trajectories of the electrons that emerge from the emitters, travel in the RF fields of the cavity, and impact the RF surface. The

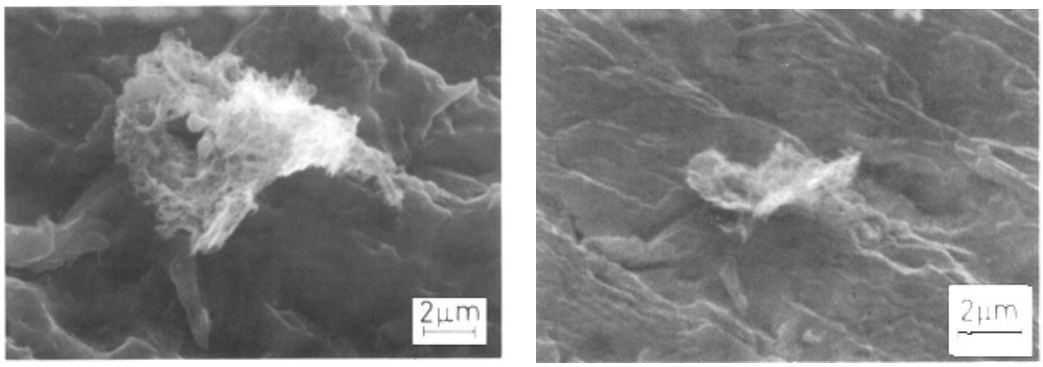

(a) (b)

FIGURE 1. (a) A carbon particle emission site (b) same as (a) but viewed at a different angle.

power deposited by the impacting electrons depends not only on the trajectory but also on the intrinsic properties of the emitter — i.e., on the field emission current. Typical $\beta_{\rm FN}$ values are between 100 and 700, and the emissive area values are between 10^{-9} and 10^{-18} m^2. The RF tests are followed by dissection of the cavity to examine and analyze the emitter with surface analytic instruments.

Both RF and DC studies reveal that emitters are micron- to sub-micron-size contaminant particles. The natural surface asperities originally envisioned are not usually found, except in isolated cases, e.g., when the surface is scratched so as to leave sharp protrusions at the edges of the scratch. Both DC and SRF studies failed to find any correlation between the physical area of the emission site and the emissive area, $A_{\rm e}$, deduced from the customary analysis of the field emission current within the framework of the FN theory.

Examples of microparticle field emitters found in DC are shown in Figure 1 [10], and Figure 2 [11, 12]. Examples of emitters found in SRF cavity studies are shown in Figure 3 [13], Figure 4 [14], Figure 5 and Figure 6 [15].

In view of the finding that emitters are microparticles, it does not seem reasonable to continue the customary practice of mechanically polishing electrode surfaces to achieve a "shiny" finish. In fact, such a procedure can even be harmful. It would leave particles of the abrasive grit embedded inside the material to be exposed later as field emitters. Sensitized by the results about the microparticulate nature of emitters, SRF cavities are now prepared under Class 100 Clean Room conditions. New approaches have been adopted to strive for an even higher level of cleanliness in cavity surface preparation, leading to fewer emission sites and better cavity performance. KEK studies [16] with high-pressure ($\approx$ 100 bar) water rinsing (HPR) show a factor of a hundred reduction in particle count on silicon wafers prepared under dust-free conditions of a Class 100 clean room (Figure 7). DC field emission studies at Wuppertal [17] on $\approx$ cm^2 samples also show that the density of emitters

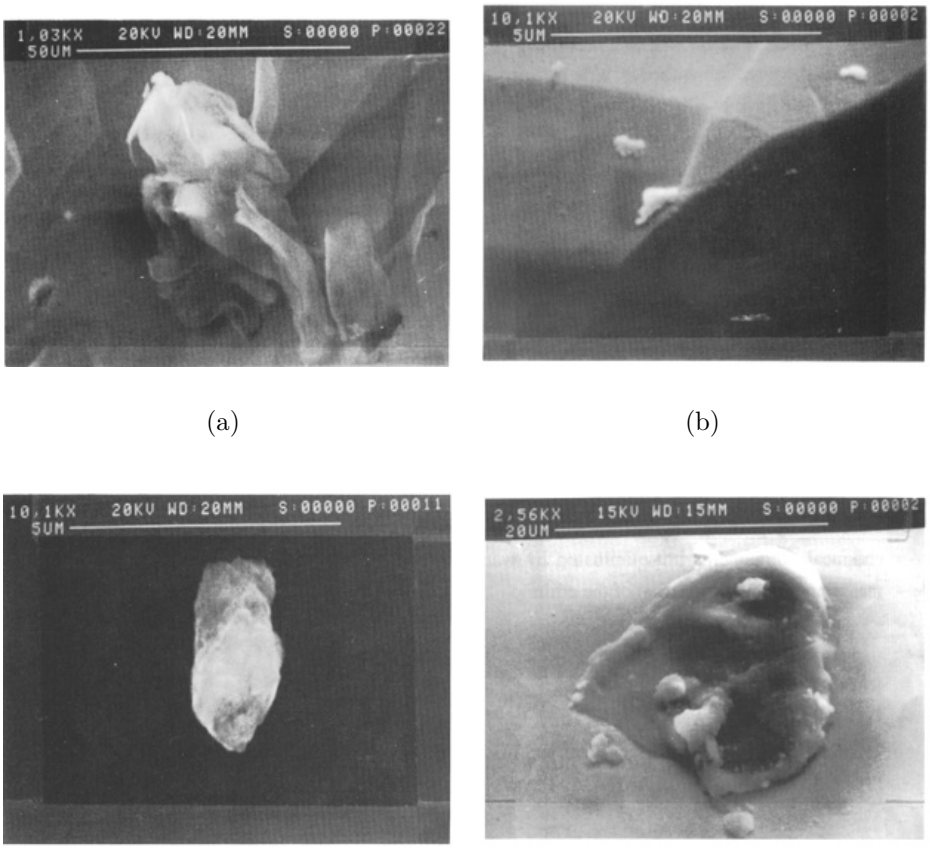

(a) (b)

(c) (d)

FIGURE 2. Microparticle contaminants found at field emitter locations. Foreign elements found were (a) C, N, O, (b) Ag (c) Si, O, (d) Ni

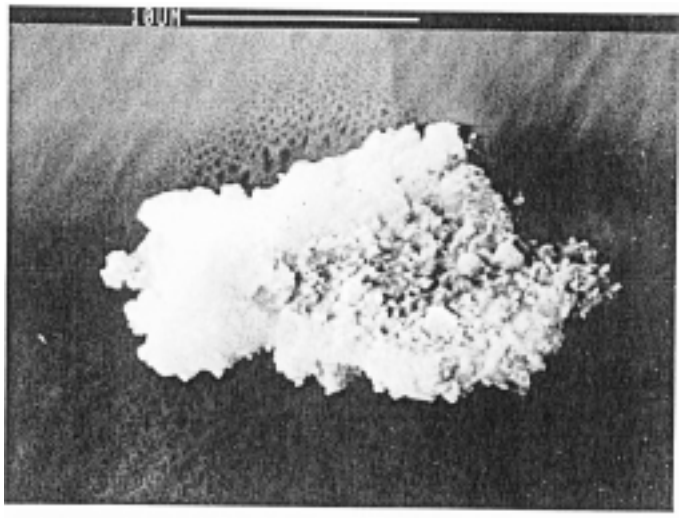

FIGURE 3. SEM photograph of a field-emitting particle located by temperature mapping and dissection of a single-cell 3000 MHz cavity. EDX analysis showed the particle to contain titanium, carbon, oxygen, sodium, indium, aluminum and silicon.

FIGURE 4. SEM micrograph of an indium metal flake field emitter. A small melted region can be recognized by its spherical shape. The particle was subjected to a maximum electric field of 26 MV/m in the RF test of the 3 GHz cavity in which it was found.

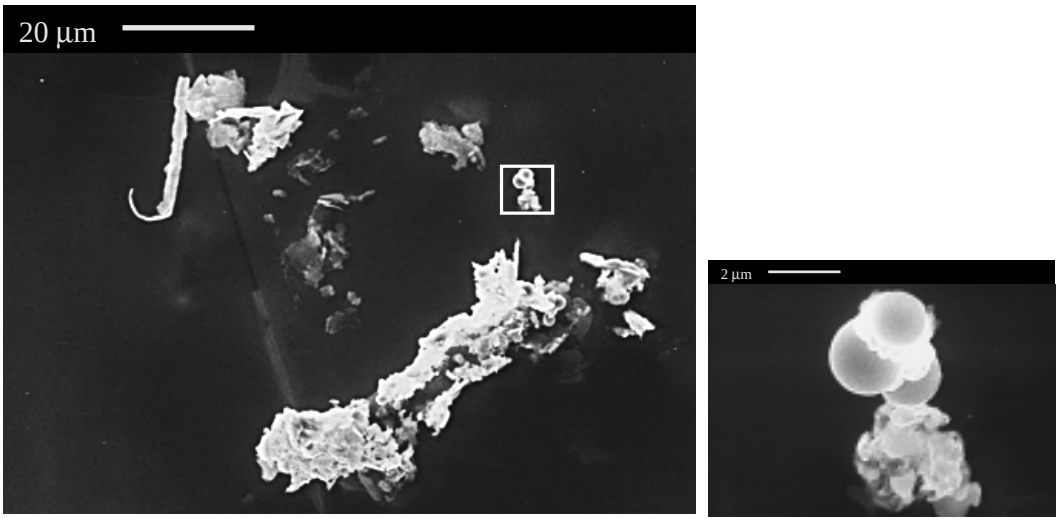

(a) (b)

FIGURE 5. (a) SEM micrograph of stainless steel emitting particles. Note the cluster of small spherical balls in the framed portion which indicate that a part of the site melted. (b) The melted cluster is expanded. EDX analysis show that the particles are stainless steel.

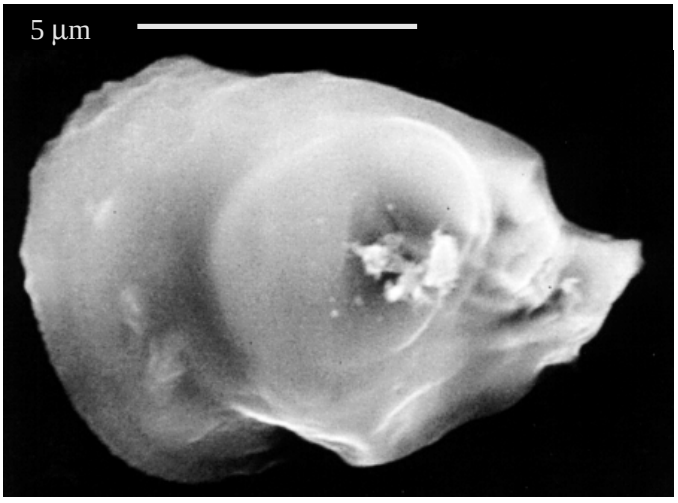

FIGURE 6. SEM photo of a relatively smooth emitting particle found in a single-cell 1500 MHz cavity by temperature mapping and subsequent dissection. EDX analysis showed the particle to contain carbon, oxygen, iron, chromium, and nickel.

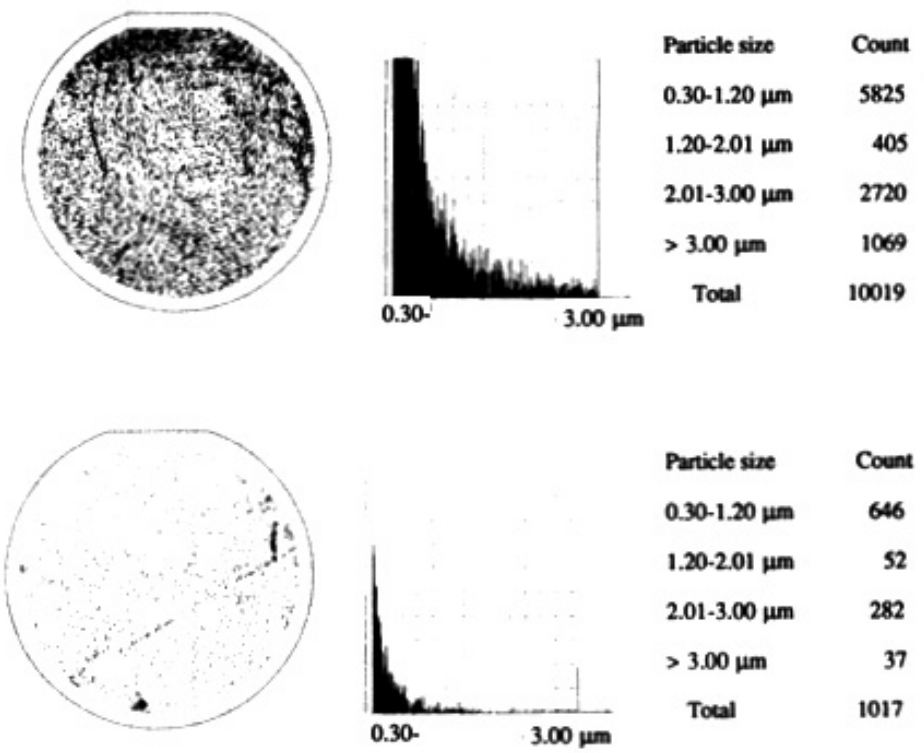

FIGURE 7. (a) A 100 cm^2 silicon wafer disk prepared by exposure to standard chemicals and cleaning techniques used for superconducting cavities shows a large number of contaminant particles detected by a laser scanner. (b) The same disk, after high-pressure rinsing, shows a substantial reduction in particle count.

is reduced by HPR.

Although all emitters are found to be associated with microparticles, it is remarkable that not all micro-particles turn out to be field emitters. Only about $5 - 10$ % emit at fields less than 100 MV/m. Figure 7(a) shows an enormous number of foreign particles found by laser scanning on the silicon disk which was exposed to SRF cavity treatment chemicals outside the clean room, rinsed with high purity filtered water used to clean niobium cavities, and dried in a Class 100 dust-free clean room. The aim of the study was to expose the disk to the same environment as the cavities. There are more than 100 particles per cm^2 of sizes between 0.3 to 3 μm. Following a similar line we examined several samples of niobium etched for 30 - 40 minutes, rinsed and dried in a Class 100 clean room [18]. We searched with the SEM for particles larger than 1 μm over an area of a few mm^2 on each sample. The average density of particles we found was 350 per cm^2 over five samples, not inconsistent with the density found from the laser scanned silicon disk studies conducted by KEK.

Now consider the density of field emission sites found in SRF and DC studies as shown in Figure 8. Both the cavity and the samples for DC study were prepared

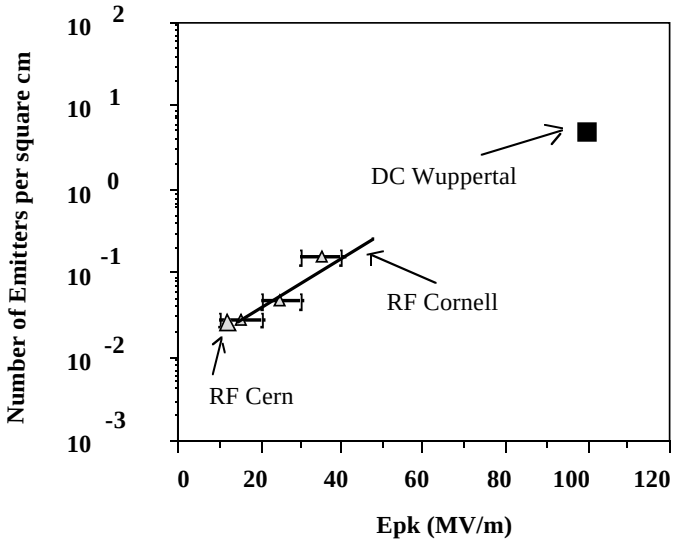

FIGURE 8. Density of field emission sites identified in DC (Wuppertal) and RF studies (CERN and Cornell).

in Class 100 clean room. There is an encouraging consistency between the density of emitters found in DC and RF studies. There are only 0.1 emitters per cm^2 at 30 MV/m rising exponentially to 10 emitters per cm^2 at 100 MV/m.

Even at 100 MV/m, the number of emitters is far smaller than the number of micro-particles. Another way to describe this situation is to say that the $\beta_{\rm FN}$ value of most particles is well below 50. What makes some of the microparticles into emitters and some not? What is the mechanism that gives rise to observed $\beta_{\rm FN}$ between 50 and 700? The present thinking is that, besides the microparticle, there are additional physical aspects that play important roles in determining whether a particle will be a field emitter:

1. The detailed geometry
2. The condensed gas adsorbates
3. The interaction between the particle and the insulating layer on the surface.

This is a rich subject with many experimental findings as well as creative models proposed to account for such findings. We will present one item of evidence for each aspect listed above to show the reason to believe that such aspects do indeed play a significant role.

A Geometry of the Microparticle

In a definitive DC field emission experiment conducted at Saclay [19], with intentionally introduced particles, it was found that smooth spherical particles of iron or nickel do not emit, but jagged particles emit strongly. One example each

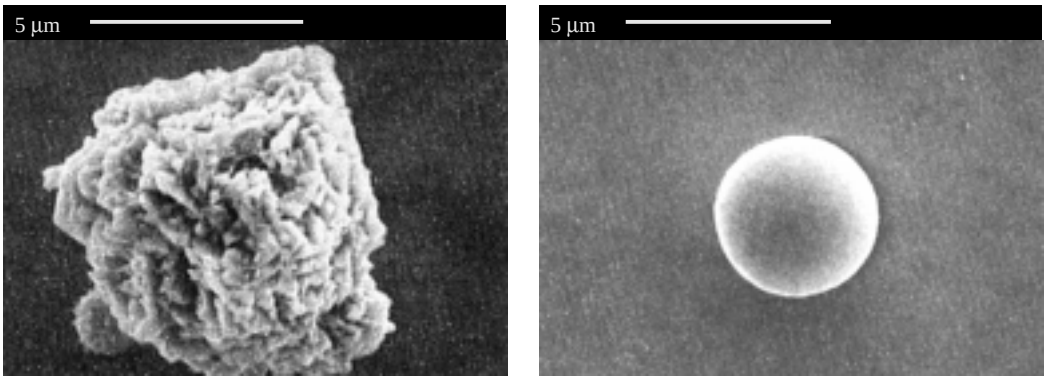

(a) (b)

FIGURE 9. SEM micrographs of two intentionally introduced nickel particles from a field emitter study: (a) jagged shape and emitting (b) smooth and non-emitting up to 100 MV/m.

of a smooth and a jagged particle is shown in Figure 9. Iron particle emitters are frequently found in cavities. Therefore, iron is a suitable candidate for artificial emitter studies. The experiment shows that microgeometry plays an important role in field emission.

A simple interpretation for the mysteriously high value of β_{FN} would be that the particle as a whole enhances the field by $\beta_1 \approx 10$ and smaller protrusions on the particle further enhance the field by $\beta_2 \approx 10$. The product $(\beta_1\beta_2)$ is sufficient to explain observed values of $\beta_{\mathrm{FN}} \approx 100$. The jagged structure of the indium particles and the stainless steel particles shown in 4 and Figure 5 corroborates the simple geometrical field-enhancement interpretation. The microtip features also offer a simple explanation of current instabilities; namely, when one tip melts (from ohmic heating due to the field emission current) and becomes smooth, the local β_{FN} value decreases, and emission from another tip takes over. However, the microgeometry model is hard pressed to account for β_{FN} values much larger than 100.

B Condensed Gases or Adsorbates

There is good evidence to show that emission sites can be activated by condensed gas. An SRF cavity was exposed to a steady stream of oxygen gas while the cavity was cold. Before exposure, the cavity was measured to be emission free by the temperature map of Figure 10(a). When the oxygen was introduced, most of the gas probably condensed on the vacuum pipes, but some reached the cavity surface, as evidenced by a sudden increase in field emission. The temperature map of Figure 10(b) shows a strong emitter activated by the condensed gas. To rule out the possibility that the new emitter was just a new particle, introduced accidentally with the oxygen stream, the cavity was cycled to room temperature. On returning

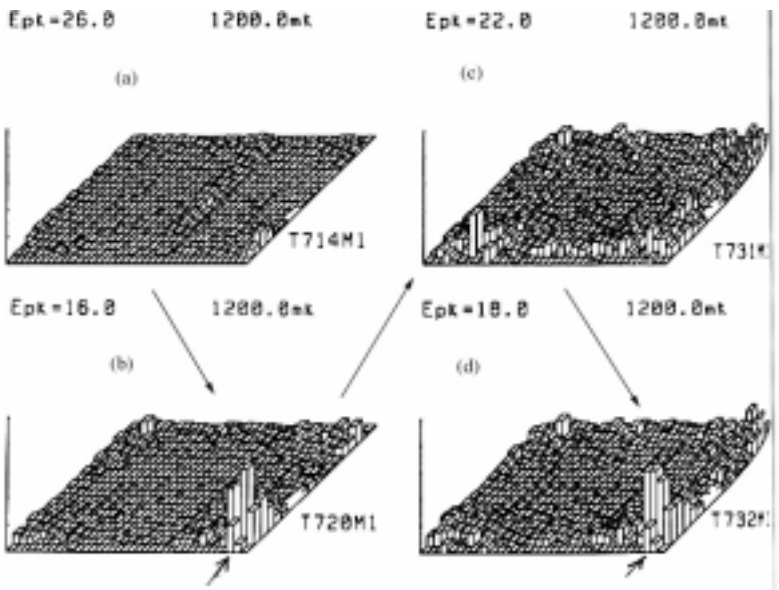

FIGURE 10. (a) Temperature maps of a 1500 MHz cavity. (a) The surface is emission-free at 26 MV/m. (b) Emitters appear when the cavity is exposed to oxygen. (c) Emitters are no longer active after cycling to room temperature. (d) The same emitters reappear when exposed to oxygen a second time.

to 2 K, emission at the previously activated site was absent. However, readmission of oxygen reactivates the *same* site. It is highly unlikely that a particle would land on the same spot during two separate doses of gas.

There are theoretical models [20] to show how emission properties can be amplified by a superficial layer of absorbed gas. The presence of an adsorbed atom (adatom) can give rise to "resonant tunneling." The large range of A_e values observed for emitters may be due to a variety of condensed gas species and condensed layer thicknesses.

C Interface

Results from field emission studies that involve heat treatment [10, 17, 21] suggest that the interface between the particle and the substrate may also play an important role in whether a random microparticle becomes an emitter. As shown in Figure 11, heating a Nb surface with emitting particles to 1400 °C renders the surface emission-free. In some cases, the responsible particles also disappear, presumably by evaporation or dissolution. But, in other cases the original particles are still found to be present on the surface. One may argue that the jagged edges on the surviving particles are made smooth by heating to 1400 °C. However, the surprising result is that heating an *emission free* Nb surface to temperatures between 200 °C and 600 °C converts some nonemitting particles into emitters. It is unlikely that heating to 200 °C will make a smooth particle into a jagged one.

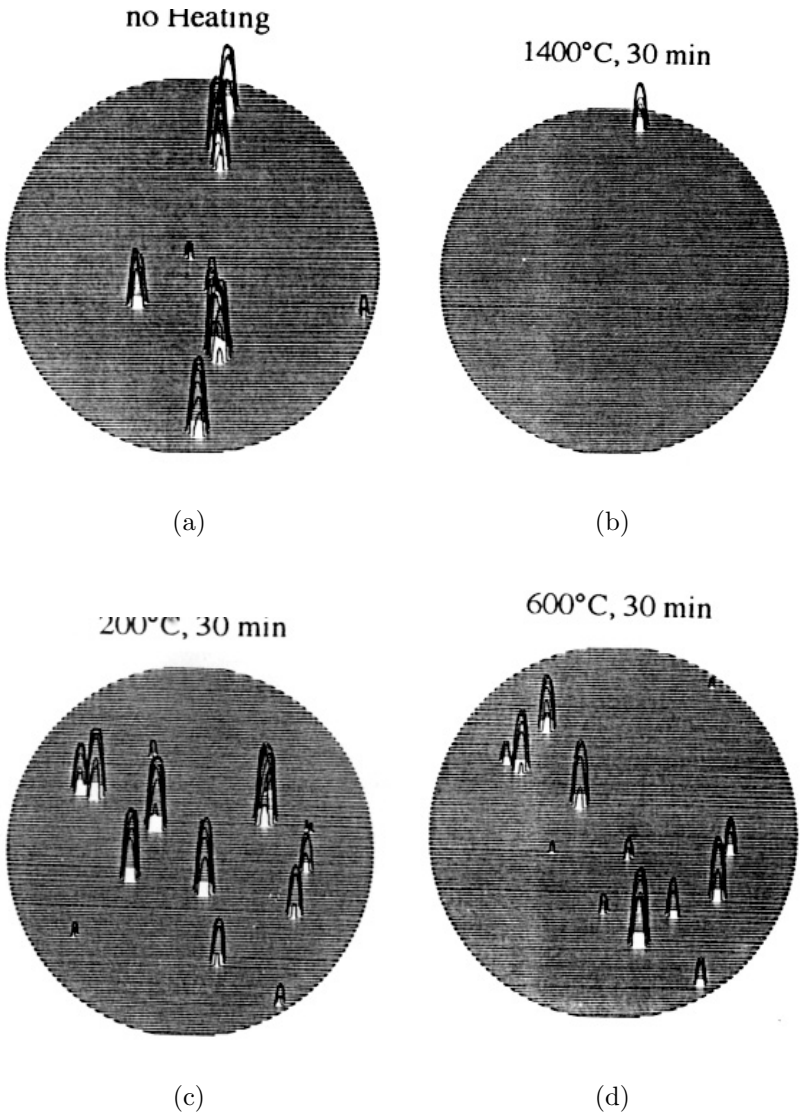

FIGURE 11. DC field emission scans to study the effect of heat treatment on emitters. In these plots, the emission sites are represented by two-dimensional peaks. (a) Without heat treatment. (b) An emission-free niobium surface obtained by heating to 1400 °C. (c) Reheating a 1400 °C treated field emission-free surface to 200 °C. (d) Reheating a 1400 °C treated field emission-free surface to 600 °C.

One possible explanation for the new activation is that the interface between the particle and the underlying surface is affected by the heat treatment. Another possibility is that reheating produces new adsorbates; for example, excess sulfur was found on newly activated sites [10]. We still need a clearer understanding of the influence of the interface and adsorbates on β_{FN}. The Aston group [22] has

proposed several models which involve an insulating interface between the emitter and the base metal.

II THE PHYSICS OF EMITTER PROCESSING DURING VOLTAGE BREAKDOWN

When raising the RF electric field in a superconducting cavity with a freshly prepared surface, the field emission often decreases abruptly; the cavity is said to "process" or "condition". Temperature maps show that individual emitters extinguish during such processing events. Much progress has been made in subsequently characterizing the processed emtters at a microscopic level using surface analysis techniques such as SEM, EDX, and Auger.

A processing event [14] is shown in Figure 12. The temperature map shown in the upper panel recorded the original field emission. At about $E_{\rm pk} = 29$ MV/m, when the incident RF power was increased, the peak field in the cavity jumped to 39 MV/m. The lower panel of Figure 12 shows a temperature map taken after the processing event. A comparision of the two maps shows that the field emission heating is substantially reduced at 29 MV/m. Upon dissecting the cavity and examining the predicted location in the SEM, the site shown in Figure 13 was found. The 200 μm site has a "starburst" shape with a 10 μm molten crater-like core region accompanied by micron-size molten particles within and near the crater. EDX analysis shows that the starburst region and the molten crater are all pure niobium, within detection limits. The particulate matter in the crater region, visible more clearly in the expanded Figure 13(b), reveals copper as the only contaminant. Presumably, a μm-size copper particle was originally responsible for the field emission.

The molten crater and splash-type features at the edges of the crater make it clear that emitter processing is an explosive event. As we will show, there is good evidence that the explosion is the result of a micro-discharge, also referred to as an RF spark or an arc. The fact that the event can melt niobium on the cold surface suggests that the explosion takes place on a time scale much shorter than the thermal relaxation time.

It is important to emphasize that, after the explosive discharge, the field emission decreased and higher field levels were reached, despite the appearance of craters and molten droplets surrounding the craters. This is not surprising in view of the fact that studies at Saclay show that smooth particles do not emit.

A Craters

Several hundred starburst/molten crater sites have been examined with SEM/EDX by dissecting SRF cavities tested to high fields. In general, the higher the RF electric field, the larger the number of starbursts/craters found. We show a

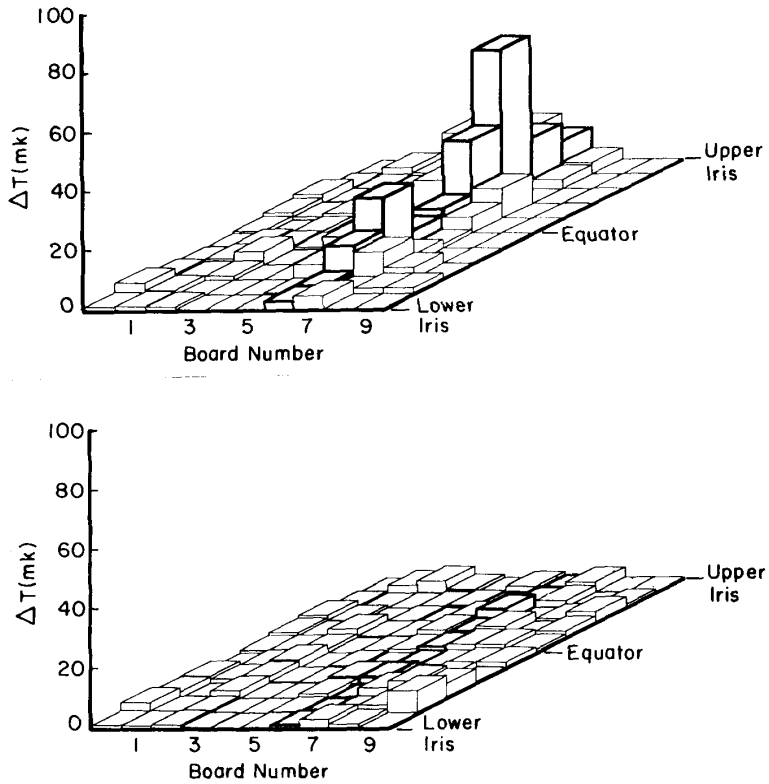

FIGURE 12. (Above) Temperature maps at 29 MV/m before the processing event. (Below) After the processing event, again at 29 MV/m.

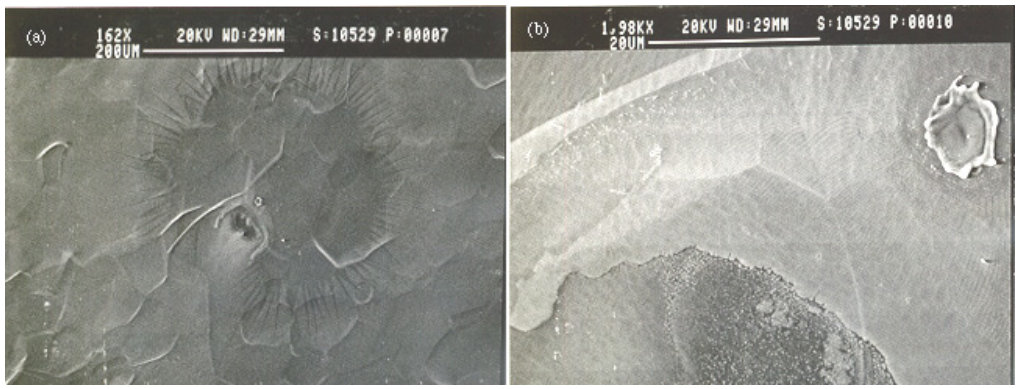

FIGURE 13. SEM pictures of the processed site found at the location predicted via temperature maps. (a) Low magnification and (b) high magnification of the crater region within the starburst of (a). A particle at the center of the molten crater as well one outside the crater were found to contain copper.

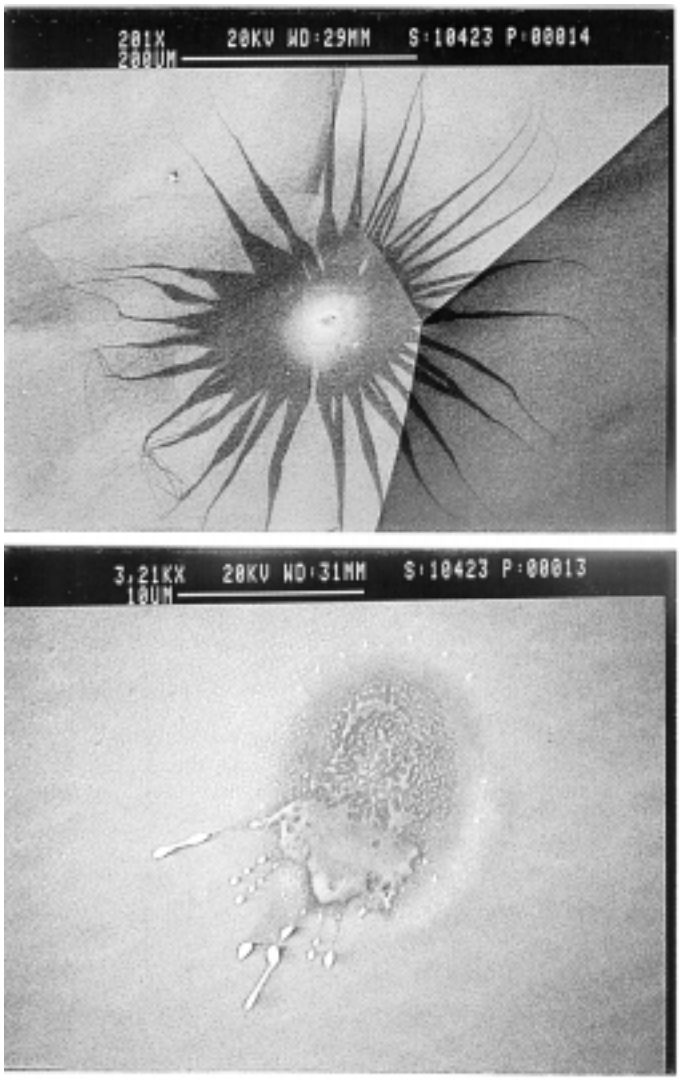

FIGURE 14. (Upper) Starburst with (Lower) central indium crater

few more examples of starburst/crater sites. One has melted indium in the crater (Figure 14); one has melted stainless steel in the crater (Figure 15). Figure 16 shows another starburst/crater site with molten copper particles near the central crater. When molten particulate debris is found near and around the craters, it can usually be analyzed by EDX.

It is often the case that EDX can detect no foreign elements in or around the crater region, only molten niobium. But with the more surface-sensitive Auger method, we can detect thin layers of foreign metals inside most craters. Auger analysis results of Figure 17 shows a crater with a thin film of iron coating the crater. Figure 18 shows a film of copper and indium covering a crater region. Most of the impurities are seen within 2 or 3 crater radii of the crater center [23].

Although Figure 13 to Figure 16 show single craters from processing events, it

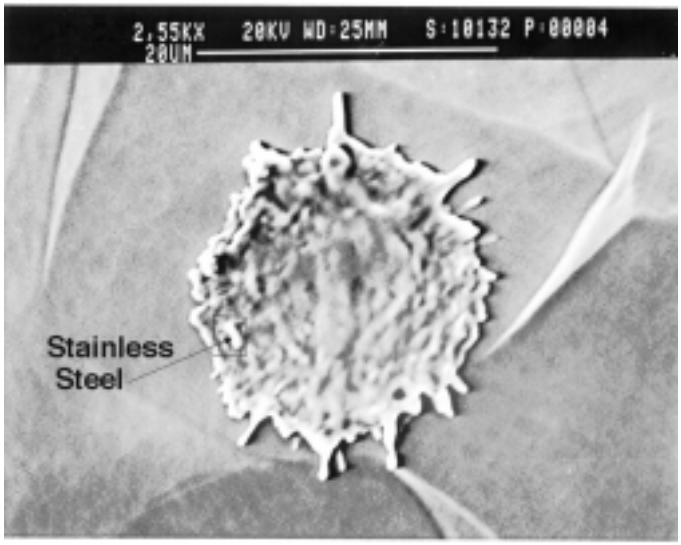

FIGURE 15. A crater with a melted particle of stainless steel

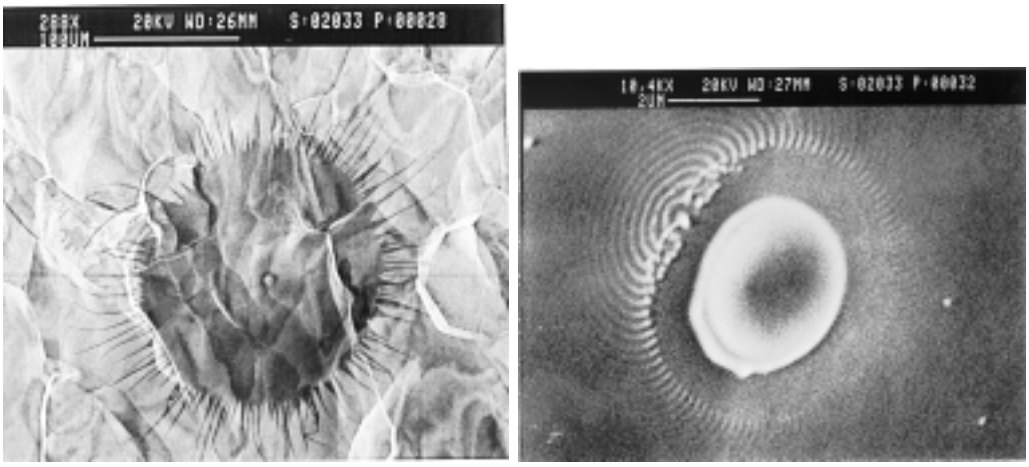

(a) (b)

FIGURE 16. SEM micrographs of a processed emission site. (a) Large starburst with single central molten crater. (b) The expanded molten crater region shows sub-micron size melted copper particles, presumably from the original copper emitting site.

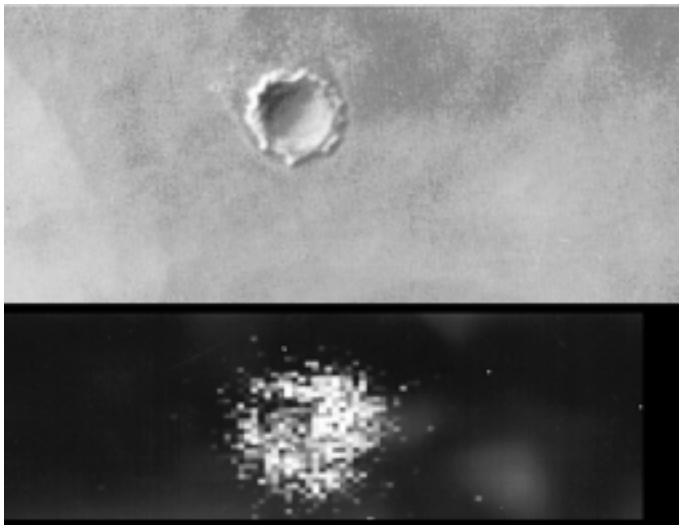

FIGURE 17. A crater with a thin coating of iron. (Upper) SEM micrograph (Lower) 2-D Auger scan of crater region.

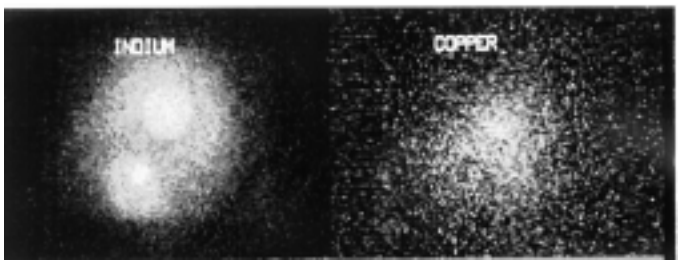

FIGURE 18. A crater with a thin coating of indium and copper detected by Auger analysis. (Left) Indium (Right) Copper. Both coatings were found on the same crater.

is more usual to find multiple craters. These can be a cluster of craters, a track of craters, a large number of chaotically overlapped craters with ripples emananting from the craters. Figure 19 describes a rich variety of crater patterns discovered.

Both single and mutliple craters have been found in copper RF cavities after high-power conditioning to reach very high surface fields. Extensive tests have been carried out at SLAC [24] on 3 GHz and 11.4 GHz copper cavities using high power (50–100 MW) pulsed (μsec) RF. Record surface electric field levels between 200 and 600 MV/m were reached after many tens of hours of conditioning. Subsequent visual inspection of high field regions shows numerous crater areas, with many overlapping craters. After processing to very high fields (200 MV/m) the entire iris is pock-marked by overlapping craters.

Craters and molten areas have also been observed in DC emission studies, when vacuum breakdown with a high DC voltage results in arcing. Extensive studies have been performed in DC, and comprehensive reviews are available [8]. As with cavities, the craters found in the DC studies have characteristic sizes on the order of microns. There are often multiple overlapping craters.

DC field emission studies using very short pulses show that spark formation times are between 10^{-9} and 10^{-6} s. In such a short time scale, the emission site is thermally isolated from the surface. As a result, it is possible to find molten metal in superconducting cavities which operate at liquid He temperatures. It is reasonable to surmise that the processing of emitters in superconducting cavities also results from vacuum breakdown and is accompanied by an arc, or spark, produced by the RF electric field. We frequently refer to this event as a microdischarge because it is localized near the emitter.

B Studies of the Same Particles Before and After Explosion

So far we have shown that emitting particles (Figure 4 and Figure 5) and exploded craters (Figure 14 and Figure 15) have common elements. The presence of the same elements in emitting particles and exploded craters indicates that emission from micro-particles eventually evolves into an explosion during the microdischarge. To strengthen the correlation between the original emitting particle and the final explosion we have obtained *before explosion/after explosion* micrographs of the very same particles. Figure 20 and Figure 21 show "before/after" pictures of two groups of carbon sites which exploded in an RF field. The carbon particles were introduced by touching the RF surface with a sharp "number two" pencil. The "after" pictures were taken following the RF test during which the host cavity reached an electric field of 60 MV/m at the region of the intentially deposited carbon flakes. A comparision of the topography of the niobium grains in the upper and lower parts of each figure assures us that we are looking at the same region before and after the RF test. For each group of carbon flakes seen in the lower panels, the corresponding upper panels show the results after the RF test. The

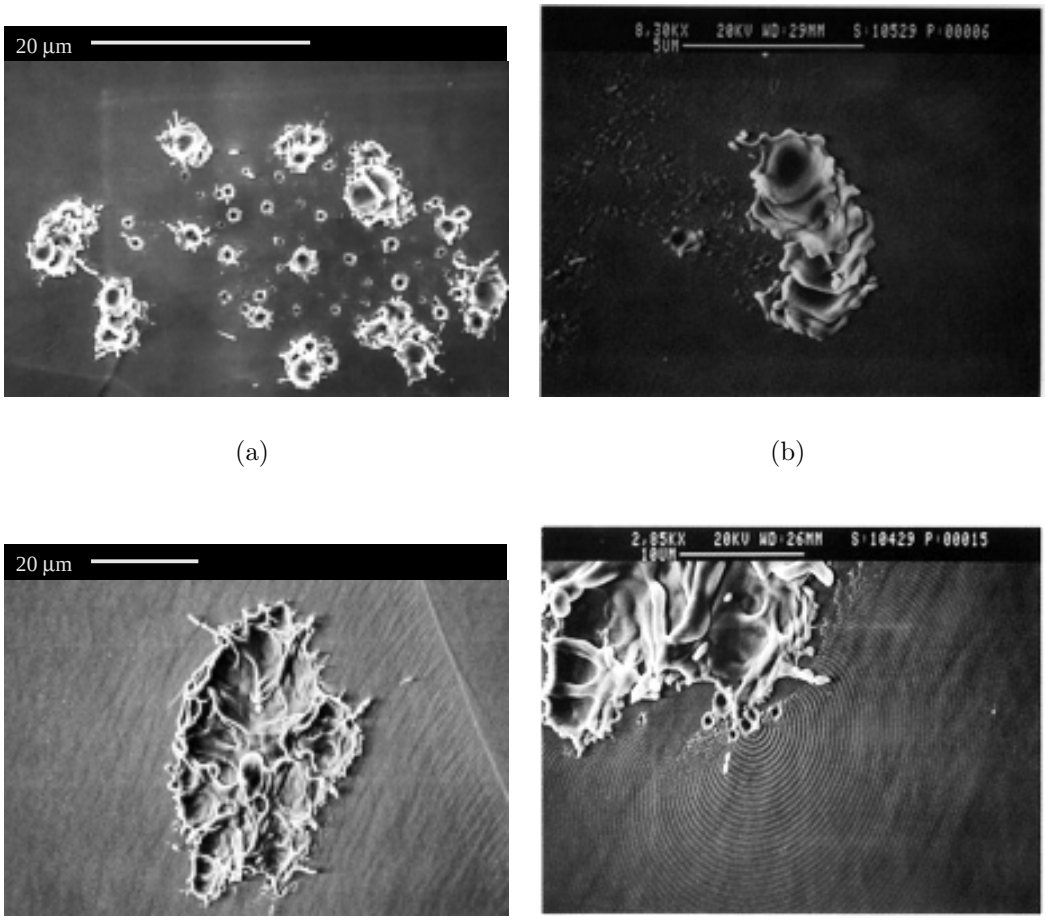

(a) (b)

(c) (d)

FIGURE 19. SEM micrographs of a variety of crater patterns found in processed emission sites (a) A cluster of craters seen as a tight ensemble about a central point. (b) Crater tracks suggesting a path defined by a sequence of craters. (c) Chaotically overlapped craters. (d) Ripples emerging from molten craters.

entire region covered by carbon flakes before the test is covered with craters after the test.

It is interesting to note that when EDX analysis was applied to the craters it could not identify any of the original carbon. As we mentioned before, EDX analysis is just not sensitive enough to discern thin layers of foreign material coating that may nonetheless be present and can be identified with Auger analysis. We presume that the activity during the explosion of the carbon flakes is intense enough to vaporize the original microparticles. We did not carry out Auger analysis on the carbon regions after the RF test.

Even though the presence of a large number of craters at the location of the carbon flakes provides strong evidence that the flakes were the cause of the craters, it would be much more satisfying to produce the explosion of a *single* particle that is well characterized before the RF test. Proceeding along these lines, we developed special techniques to deposit a *single particle* of silica on an RF surface. Figure 22 shows the original particle of silica *before* the RF cold test [25]. After testing the host cavity to 75 MV/m, Figure 23 shows the region of the silica site *after* the RF test. To the best of our knowledge, this is the first time a micro-particle has been characterized both *before and after* its explosion. The site has a multiple "starburst" shape extending over a 100 μm . There is a 10 μm molten crater-like core region in the expanded micrograph of the lower panel. EDX could detect no foreign elements at this site. As mentioned, this is not surprising because of the limited sensitivity of the EDX method.

C The Nature of Starbursts

There are many interesting aspects about starbursts that reveal some of the physics underlying the microdischarge and emitter explosion. The starburst has turned out to be a convenient means of locating processed sites because of its large size, typically 100–500 μm as compared to craters which are 1–10 μm. The starburst pattern is discernible only in the SEM and not visible in an optical microscope. Another interesting aspect about the starburst is that it tends to fade away after a few hours of air exposure, but it is stable in a vacuum or a dry nitrogen atmosphere. Of course, the molten craters remain unaltered on exposure to air. These facts show that the starburst is a very subtle modification of the surface - perhaps only a few monolayers deep.

Auger studies shed further light on the nature of the surface modification [23]. Comparing Auger spectra inside and outside a starburst, fluorine is found outside, but not inside. A 2-D fluorine map (Figure 24) of the surface near the starburst clearly showed a good overlap between the geometric shape of the starburst and the region of fluorine depletion. Following argon sputtering of the surface, we determined that the fluorine layer present everywhere on the niobium surface was at least 50 Å deep, but not more than 1500 Å. Fluorine presumably comes from the HF in the acid etching solutions used to prepare the niobium cavity surface for

FIGURE 20. (Lower) SEM pictures of a cluster of carbon particles located on the surface of a cavity before the RF test. (Upper) After the RF test the region was covered with craters. The field at the region during the RF test reached about 60 MV/m.

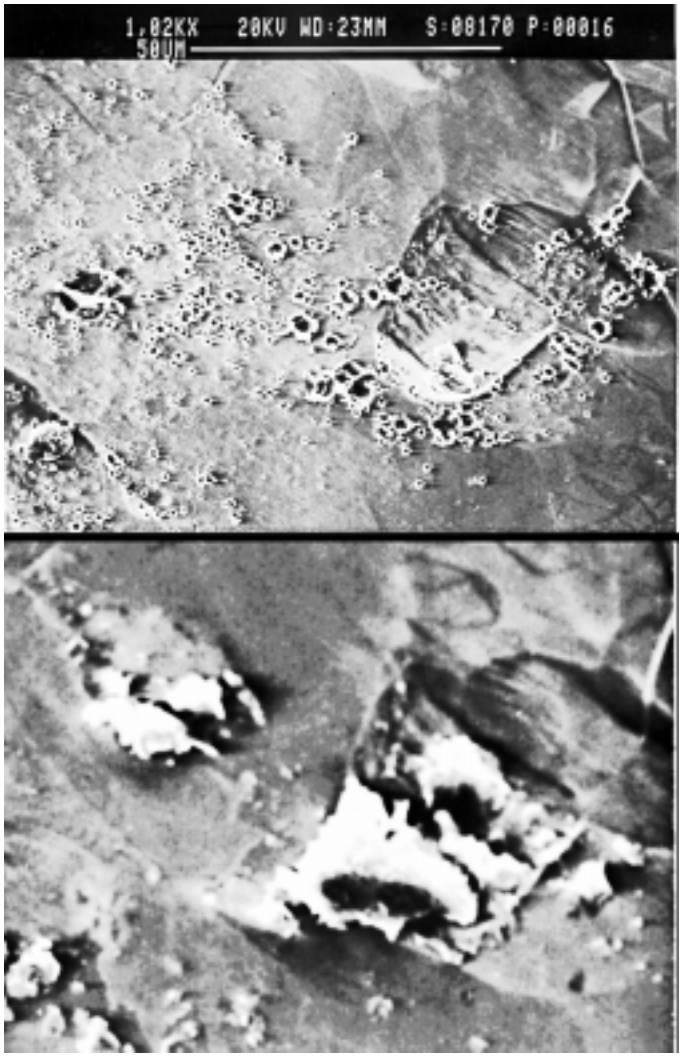

FIGURE 21. (Lower) SEM pictures of a second cluster of carbon particles located on the surface of a cavity before the RF test. (Upper) After the RF test the region was covered with craters. The field at the region during the RF test reached about 60 MV/m.

FIGURE 22. SEM picture of a field-emitting particle located on the surface of a cavity before the RF test. After the test this particle was found to be exploded, as shown later. The white grain-boundary line at the lower right corner serves as a fiducial for the location of the particle.

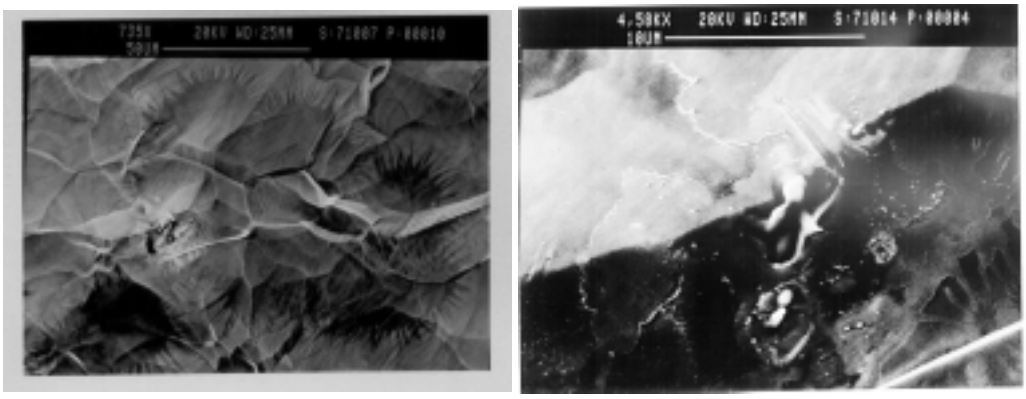

FIGURE 23. SEM micrographs of a processed emission site. (a) SEM picture of the silica particle after the RF test. (b) Expanded SEM picture of the sparked silica particle. Here we see the molten crater region in more detail. The white grain-boundary line at the lower right corner assures us that the melted region is identical with the location of the original silica particle.

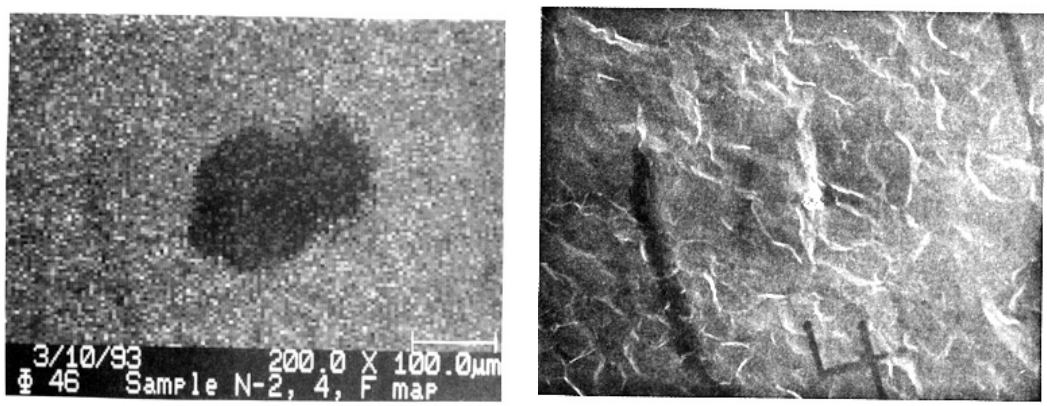

(a) (b)

FIGURE 24. (a) A two-dimensional Auger scan of a starburst region restricted to look for the element fluorine. The dark region means an absence of fluorine. (b) SEM micrograph of the same region. Note that the starburst has partially faded due to exposure to air during the time it took to transport the specimen to the Auger facility. While the sample was in the SEM, the electron beam was used to burn in a set of "brackets" around the starburst, so that it would be easier to locate the same region in the Auger system.

good RF performance.

These results suggest that the starburst pattern is formed on the niobium by the plasma cloud that develops during the spark. The superficial residue of fluorine is preferentially removed by ion or electron bombardment within the plasma. Presumably other superficial layers, such as water or hydrocarbons, may also be removed by the plasma, but these re-grow relatively fast after exposing the cavity for examination. Perhaps the surface is covered by a thicker layer of oxygen and hydrocarbons during the exposure. The high secondary electron emission coefficient of such layers eliminates the contrast and the starburst fades away.

There is evidence of intense activity inside the starburst that further support the interpretation that the starburst is related to a plasma. In Figure 25, we see both a small crater near the center of a starburst as well as several relatively large 5 μm iron particles distributed over the starburst region, all the way out to the periphery. It is unlikely that such large particles could have been ejected from the crater, considering the small size of the crater. Rather, it appears that the temperature over the starburst region was high enough to melt iron particles that were lying on the surface. One is tempted to connect this picture with Figure 5 where there are several separate particles of stainless steel lying on the surface and only a small region is emitting as indicated by the melted ball of stainless in the inset. It is quite possible that there were also several particles of iron in Figure 25 before one at the central crater exploded. The spreading starburst could have

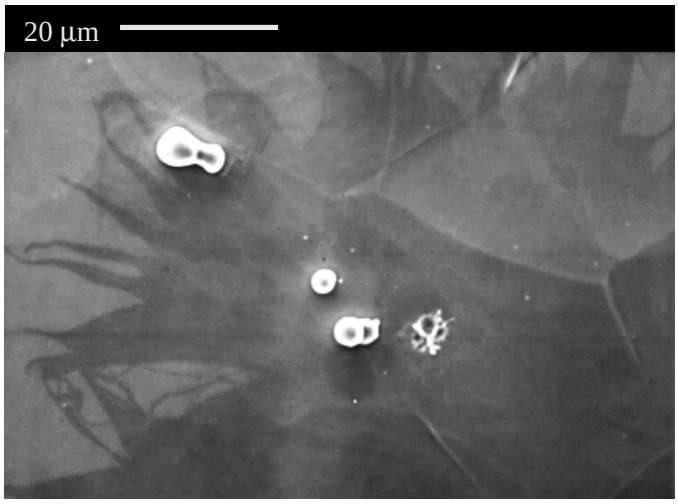

FIGURE 25. SEM micrograph of a starburst with a small molten crater. Large molten stainless steel particles located all the way from the crater to the periphery suggest that iron particles present on the surface were melted by the plasma. The temperature at the outer periphery of the starburst can therefore be quite high.

melted the others.

Examination of cathode spots during DC arcs [26–29] reveals luminous spots, attributed to the presence of a plasma. However, the starburst feature has not been reported in those DC studies. Part of the reason is that niobium is not a usual cathode material. In addition, as we explained, the formation of the starburst depends on the special chemical composition of the niobium surface. Also, starbursts tend to fade away in a few hours on exposure to air, so that the surface must be preserved in dry nitrogen or vacuum after the spark to permit the detection of thin surface modification left behind by the plasma. Our results should encourage other workers to examine cratered surfaces before allowing a long exposure to ambient air. Our Auger studies should also encourage others to examine craters with Auger to look for contaminant films that could reveal the elements present in the original emission sites.

Pursuing the close similarities in craters between RF processing and DC high-voltage breakdown, experiments were carried out to initiate a DC spark across a small gap between two *niobium electrodes* [6]. Using a field of about 100 MV/m, a millimeter-radius needle was scanned across a niobium cathode until there was a spark observed at a particular location. The gap is visible through an optical viewport. The niobium surface was prepared in the same fashion as cavity surfaces. SEM examination of the niobium cathode in the sparked area showed starbursts with molten cores (Figure 26), similar to those found in niobium superconducting cavities. This result supports the conclusion that both starbursts and craters in RF cavities are produced during a spark or microdischarge.

The gas for the plasma can come from the regions of emitter that start to melt due to ohmic heating from the FN current or from degassing of the surface near

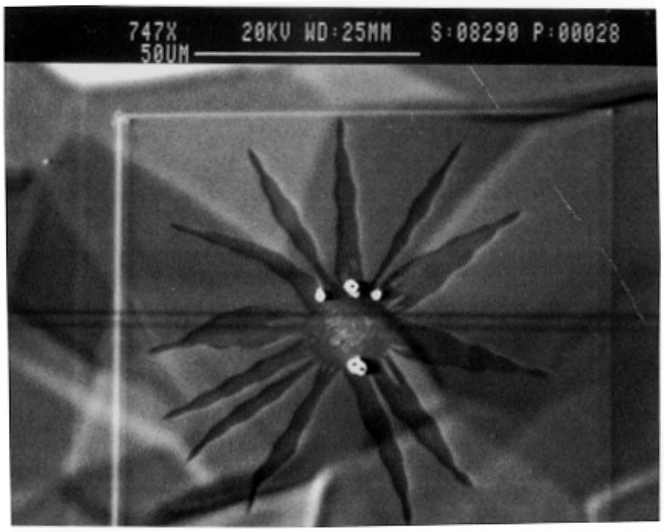

FIGURE 26. SEM micrograph of a starburst and central molten crater found on a niobium surface at the location of a DC spark at 100 MV/m.

the heated metal. Once gas becomes available, heating can intensify, since the field emission current will ionize the gas. During the part of the RF cycle that electrons are emitted ions will flow to the RF surface, depositing heat and releasing more gas. Later we will show some results of numerical simulations of such a chain of events.

The presence of gas and its subsequent ionization triggers the explosion process. Very strong support for this mechanism comes from a "helium processing experiment "[30]. The strong field emission was dominated by a single emitter as shown in the temperature map of Figure 27. This emitter did not yield to RF processing at the maximum applied RF power. Once helium gas at a pressure of about 10^{-4} torr (at room temperature) was admitted into the cavity, the emitter immediately processed, without any further increase of RF power. Upon examination of the cavity at the location indicated by the temperature map, we found the starburst and molten crater shown in Figure 28. We surmise that the addition of helium enhanced the gas density to trigger a chain of events that ultimately led to the discharge and its associated explosion and processing.

There is additional evidence to show that the plasma that resides above the emitting surface provides a strong electric field between the plasma and the RF surface and extends from the central crater out to many tens of microns. In several remarkable cases (e.g., Figure 29) we found the central crater to be surrounded by a symmetric ring of craters located about 50 microns away and within the starburst. Auger studies showed a surprising result: The satellite craters have no impurities. This observation suggests that the plasma which accompanies the explosion at a primary contaminant-loaded emission site can trigger further explosions on the Nb surface at a substantial distance away from the site without the need for any par-

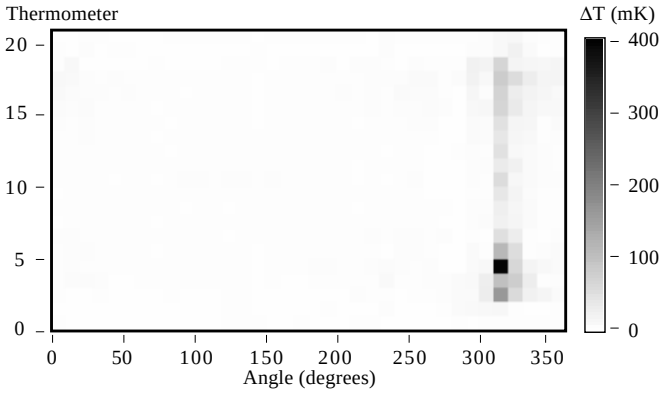

FIGURE 27. Temperature map at 17.3 MV/m showing a strong field emission site prior to helium processing. This site was completely extinguished by helium processing. The abscissa is the azimuthal location of the thermometer. The ordinate extends from the upper iris of the cavity to the lower iris.

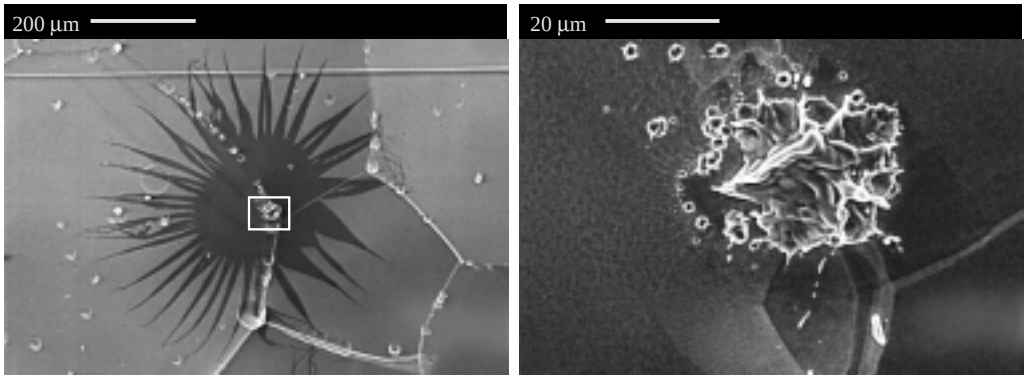

(a) (b)

FIGURE 28. SEM picture of the helium-processed site showing (a) a starburst and (b) molten craters in an expanded view. Note that (b) is rotated by about 60 degrees relative to (a).

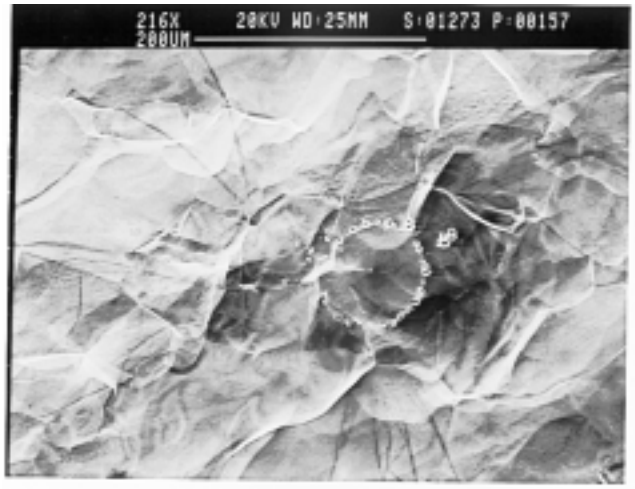

FIGURE 29. SEM micrograph of a starburst with central crater and a surrounding ring of satellite craters. The satellite craters showed no foreign elements even with Auger.

ticulate contaminants at the secondary sites. It is quite likely that the mechanism responsible for producing secondary explosions is substantial field enhancement between the plasma and the underlying RF surface. Such a mechanism also helps to explain how it is possible to form clusters of craters or a series of craters along a linear track (Figure 19).

D Incomplete Starbursts With Active Sites

In several cases we have been able to capture evidence that the plasma must form before the explosion, while the emitter is still active. We find striking examples of "incomplete" starbursts (Figure 30(a)). During the RF test, the temperature maps showed that the emitter is still active. Magnified SEM micrographs of the region (Figure 30(b)) show particles of carbon present in their non-exploded form. The presence of the raw, unexploded particles indicates that a starburst can start to form *before* the explosion that eventually destroys the emitter.

The site of Figure 31(a) shows a starburst-like feature surrounding another emitter that had not yet processed, as indicated by the temperature map. Yet another example of a starburst surrounding *an active and unexploded* site is shown in Figure 32(a). Temperature maps showed that the emitter was still active at the end of the RF test. At the increased magnification of Figure 32(b) we see a 50 μm liquefied region, with titanium and carbon as foreign elements. Clearly this large melted particle has not exploded. Unlike other processed and exploded sites, most of the contaminant particle is still intact, although a large portion of the particle is melted. The existence of such a large molten region makes it clear that the FN current cannot be the sole heating mechanism. Substantial additional heating must arise due to ion bombardment from the large cloud of plasma parked above the particle.

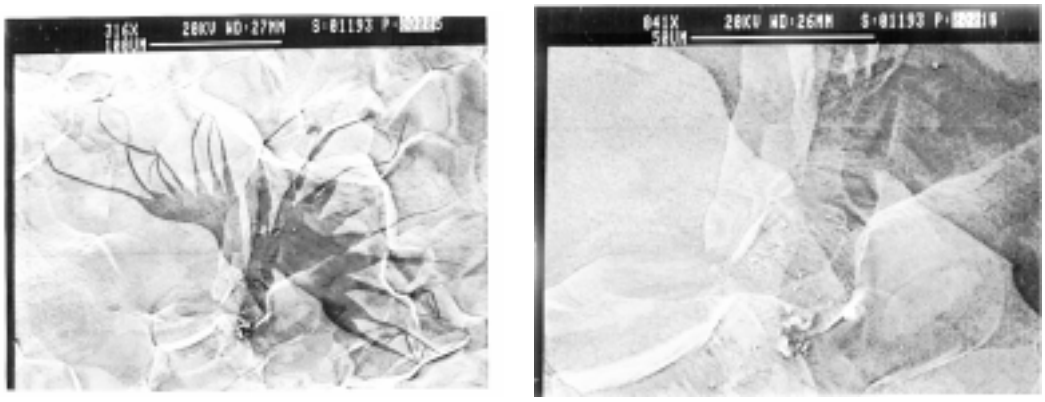

(a) (b)

FIGURE 30. An incomplete starburst with particulate debris. (a) Entire starburst region. (b) Central region, magnified showing unexploded particulate debris.

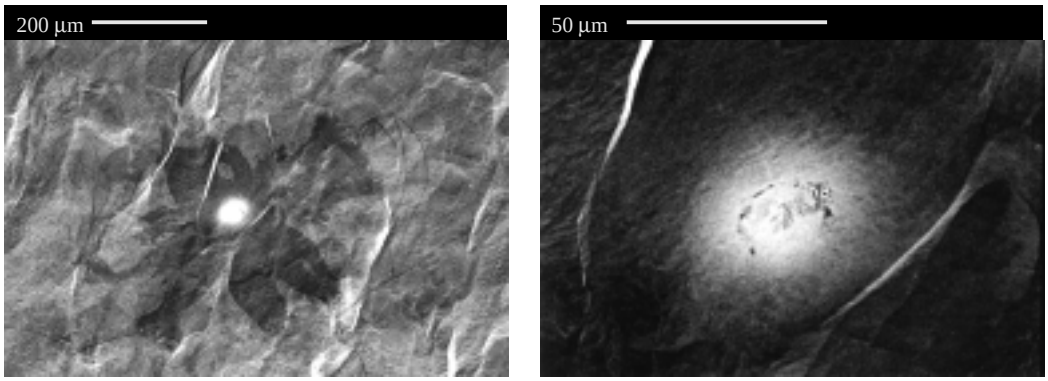

(a) (b)

FIGURE 31. An emitter active at the end of an RF test showing a dark region resembling a starburst. (a) Entire starburst region. (b) Central region, magnified.

E An Emerging Picture for Field Emission and Voltage Breakdown

The results of active emitter and exploded emitter studies have considerably improved our understanding of both field emission and voltage breakdown. There are a large number of micro-particles on the RF surface, typically 100 particles per cm^2 with sizes between 0.3 μm and 20 μm. These particles are lodged on the surface during preparation, exposed from the bulk during chemical etching, or introduced at the cavity assembly or pump-out stages.

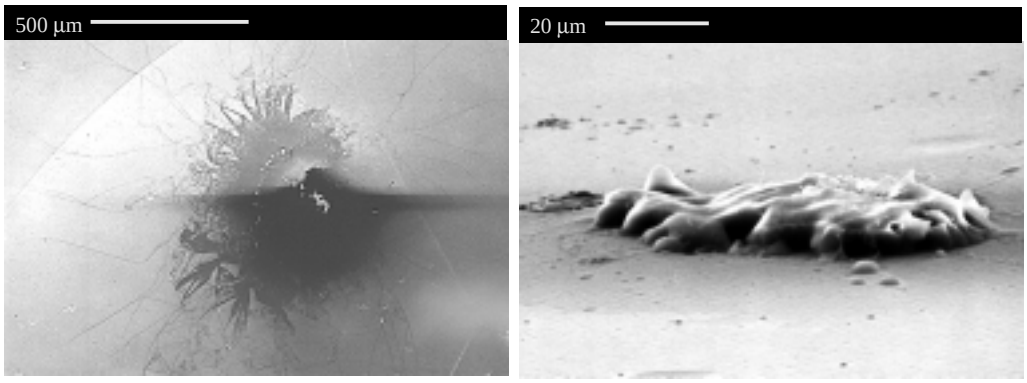

(a) (b)

FIGURE 32. (a) SEM photograph of an active emitter surrounded by an irregularly shaped starburst. The framed portion is enlarged in (b), which shows a 70 μm large particle of Ti and C that has almost completely melted, but not exploded.

Only some ($\approx 5 - 10\%$) of these particles turn out to be field emitters between 20 and 100 MV/m. Particles generally have a very irregular shape, and the microprotrusions enhance the field emission. Other important factors that influence the emission characteristics are the nature and quantity of condensed matter on the particle and the interface between the particle and the substrate. Because of these many factors it is not surprising to find a large distribution in β_{FN} and A_{e} values. Some particles that are not field emitters may become emitters later if gas adsorbs or if the interface changes.

When the field increases and the emission current density exceeds a threshold (typically 10^{11} A/m^2) the temperature at the emission region becomes high enough to melt a small region of the particle. A microprotrusion of the emitting particle may melt and cease to emit, but the overall emission from the particle continues. The melting of individual microemitters may explain the instability of field emission current.

Atoms evaporate from the melted regions to form a cloud of gas around the emission site. Ohmic heating from the FN current can also degas surface adsorbed atoms. The presence of gas surrounding the emitter now starts to play a paramount role in the later stages of intense emission followed by the eventual explosion of the emitter. Once the field emission current ionizes the gas the ions return to bombard the emitting surface causing further gas evolution. The heating can grow intense enough to melt large particles.

To simulate the ionization of gas by field-emitted current and the attendant consequences a study was carried out [15] using the program MASK [31]. We assume an emitter with $\beta_{\mathrm{FN}} = 250$ and $A_{\mathrm{e}} = 3.4 \times 10^{-14}$ m^2 and a gas flux of 1×10^{27} m^{-2}s^{-1} from the mircoemitter resulting in a local gas density of about

2×10^{24} m^{-3} at the emitter. In using the high gas flux density we assume that emission has already progressed to the point that a part of the emitter is melted and the surface gas desorption due to ohmic heating and ion bombardment is already in progress.

At 30 MV/m, emitted electrons will gain 30 eV within a micron of the RF surface, sufficient energy to ionize the gas. A chain of events then takes place on a very short time scale (nanoseconds) with the presence of gas playing a central role. Figure 33(a) and (b) show the position and energy of the field emitted electrons after 1.25 and 2 RF periods. In the presence of a positively charged slow moving ion cloud, the field emission continues even when the electric field is zero at a time equal to exactly two RF periods. The effects of the ions on the electric field and the emission current are included in the simulation. Even a *neutral* plasma creates strong electric fields due to sheath formation. Each particle represented is a macroparticle consisting of 1000 electrons and 10 ions.

As the field emission current ionizes the evaporated and/or desorbed gas, the ions are accelerated by the field toward the emission site. Figure 34(a) and (b) shows the position and energy of the ions after 1.25 and 2.25 RF periods. The ion current produces secondary ions and electrons, and heats the site further by bombardment, so that more gas is produced. A plasma is formed extending far from the emitter. The electron and ion bombardment from such a plasma cloud must be responsible for cleaning the surface. The starburst appears dark in the SEM because it is a region cleaned by the electron and ion activity in the plasma. The absence of flourine inside the starburst also indicates the cleansing action of the plasma.

MASK simulations show that the massive ions move slowly relative to the electrons so that a significant number begin to accumulate near the emitter. This leads to a substantial electric field enhancement (Figure 35(a) and (b)). About 1.5 μm away from the emission site the field is 60 MV/m. At the emission site itself the field can approach 1 GV/m. As the field grows, so does the emission current. By the top of the second RF cycle the current has increased one order of magnitude. Soon after the start of the third RF cycle the current grows unstably, leading to the explosion (Figure 36).

Although the simulations at present cannot continue to track the emerging instability beyond about 2-3 RF periods, we can surmise by extrapolation that the rapidly increasing current will be followed by a gas discharge that we call the RF spark or the arc. At the core of the arc, the intense current can melt niobium, produce molten craters, vaporize the entire emitting particle, and leave a deposited film of the original contaminant on the crater. In many cases the discharge event leaves behind molten debris. Plasma pressure during the discharge excavates the molten zone and ejects droplets. There may be multiple arcs between the ion cloud and the niobium, resulting in multiple craters from a single original emission site. In the absence of a plasma, *the crater and other melted particles do not emit because they are smooth particles.* Thus voltage breakdown in an RF cavity reduces emission and allows higher electric fields. We are used to calling this ben-

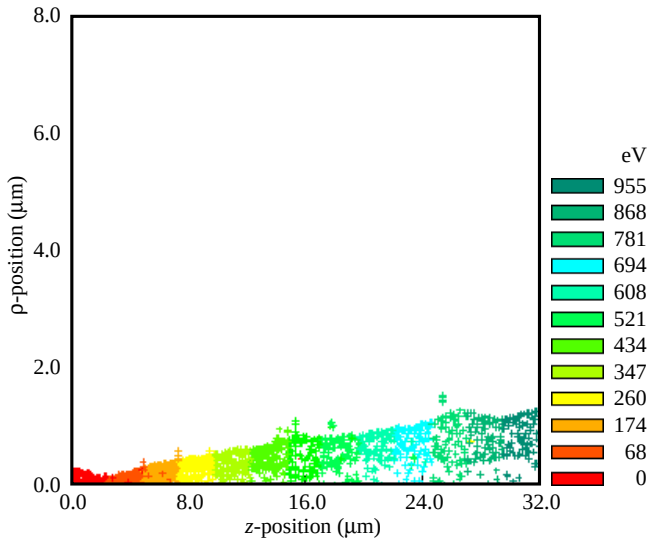

(a)

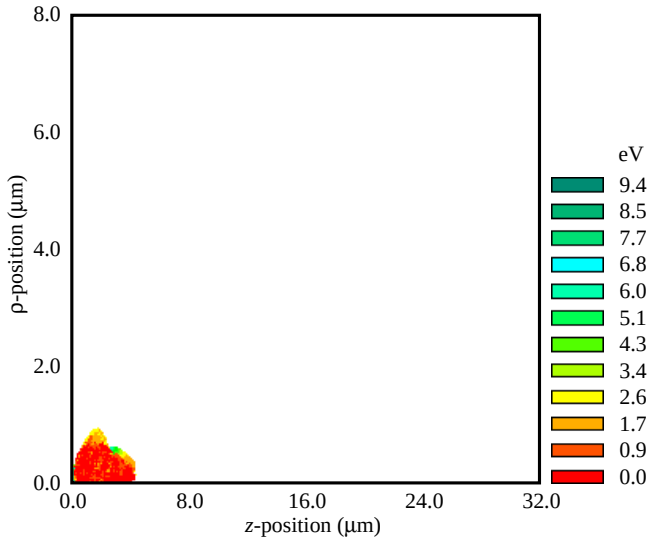

(b)

FIGURE 33. (a) Position and energy plot of electrons 1.25 RF periods into the simulation. (b) Position and energy plot of electrons 2 RF periods into the simulation. At this moment, the RF electric field is zero, yet the electron emission continues due to the electric field from the charged ion cloud.

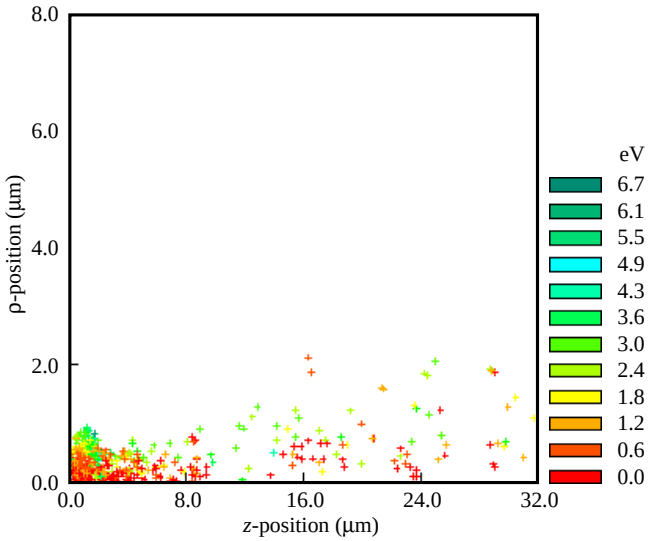

(a)

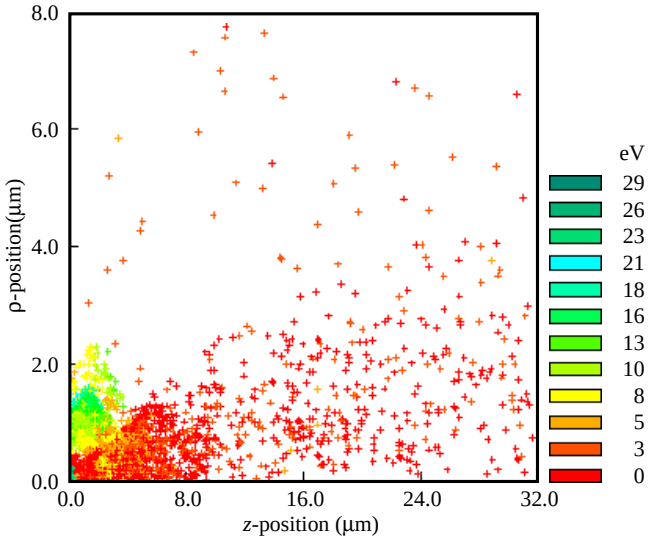

(b)

FIGURE 34. (a) Position and energy plot of ions 1.25 RF periods into the simulation. (b) Position and energy plot of ions 2.25 RF periods into the simulation.

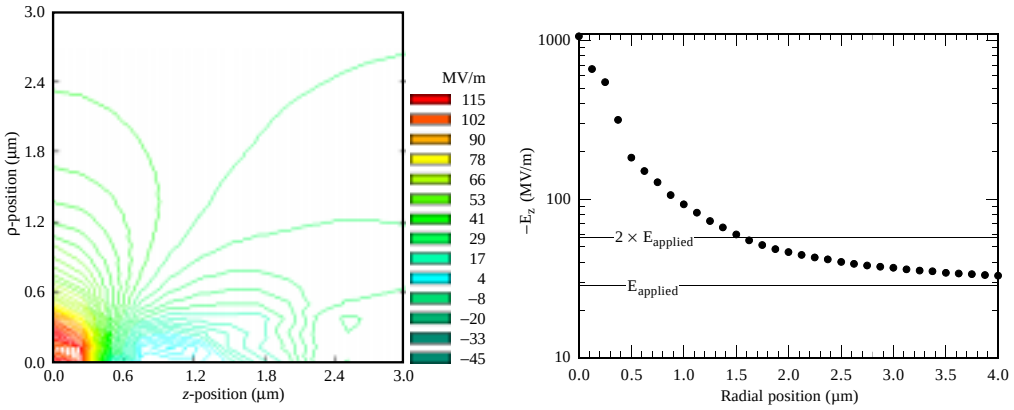

(a) (b)

FIGURE 35. (a) Contour plot of the electric field near the emitter after 2.25 RF periods. (b) Electric field enhancement due to charged ion cloud.

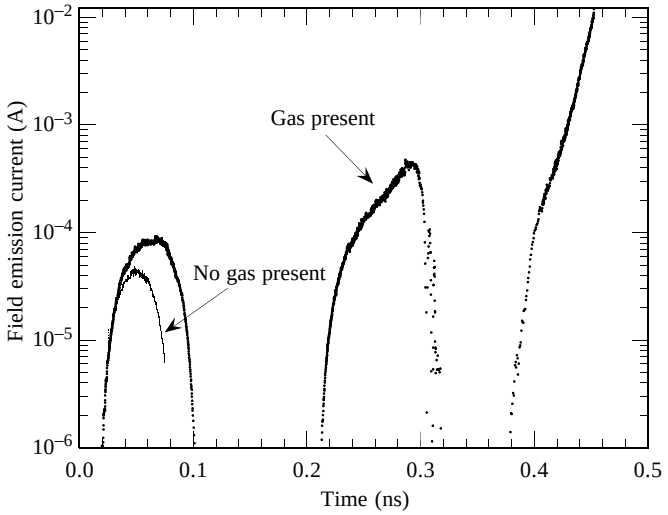

FIGURE 36. Emitted electron current versus time for two simulations, one with gas present and one without. When gas is present the positively charged ion cloud leads to a current instablility.

FIGURE 37. Chemistry and rinsing facility at the TTF.

efit "processing" or "conditioning." For a DC high voltage gap, however, voltage breakdown can deteriorate the voltage standoff capability because the spark can erode the counter-electrode and deposit more particles.

III HOW TO AVOID FIELD EMISSION

Field emitter studies discussed above show that increased vigilance in cleanliness during final surface preparation and assembly procedures is important to keep particulate contamination and associated emission under control. Figure 37 shows the care and cleanliness necessary during chemical etching and rinsing. Figure 38 shows the cavities being assembled in a clean room at the TTF.

A technique to further improve cleanliness is high-pressure water rinsing (HPR) [16], [32], [33]. A jet of ultrapure water is used to dislodge surface contaminants resistant to conventional rinsing procedures. Figure 39 shows a Cornell 500-MHz single-cell cavity for CESR under preparation for HPR. The benefits of HPR in reducing field emission are well demonstrated in tests on 5-cell cavities at CEBAF and at DESY.

FIGURE 38. Clean room assembly at the TTF.

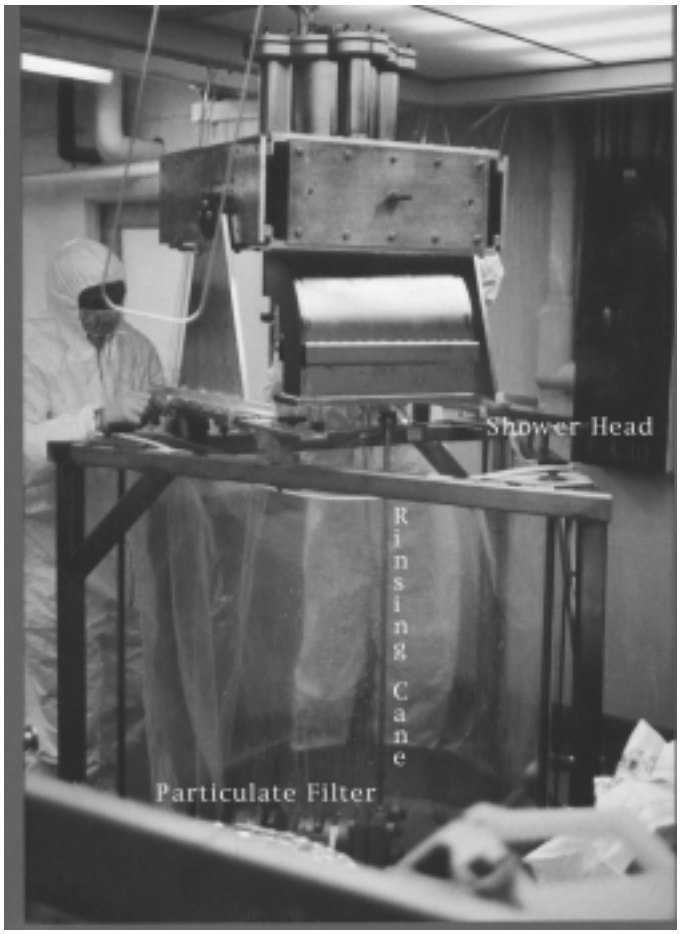

FIGURE 39. High-pressure rinsing set-up for a single-cell cavity at Cornell.

IV HIGH-POWER PULSED RF PROCESSING

The supercleanliness approach followed by HPR have both demonstrated a potential to reduce field emission. But, as temperature maps show, a single field-emission site can degrade the performance of a superconducting cavity if the emitter will not process away at the maximum RF power available. In large-area structures there is always a significant probability that a few emitters will find their way onto the cavity surface. There is also the danger of dust falling into the cavity during installation of power-coupling devices as well as during operation of cavities in an accelerator. As a result, there is a large spread observed in cavity performance. Another factor that makes the threat of dust contamination especially clear is the "area effect." At any stage in the evolution of cavity treatment technology, the maximum achieved fields decrease with cavity area.

The above remarks make it clear that a technique for eliminating emitters in situ is highly desirable for successful application of superconducting cavities to accelerators. Such a technique is high pulse power processing (HPP). It has been successfully applied to 3 GHz, 9-cell cavities [34], to 1.3 GHz 5-cell cavities [35] and to 1.3 GHz 9-cell cavities [36].

The essential idea of high power RF processing of an emission site is to raise the surface electric field at the emitter as high as possible, even if for a very short time ($< \mu$sec), as simulations and experiments indicate. As the field rises, the emission current rises exponentially to the level at which melting, evaporation, gas evolution, plasma formation, and ultimately a microdischarge (RF spark) take place. The ensuing explosive event destroys the emitter. We have discussed in detail the evidence for this model and the probable chain of events involved. Emitters have been processed away, and the field levels raised substantially. This is *not* to say that, with HPP, the need for cleanliness is eliminated. We reemphasize that to reach the highest possible field in a reproducible manner, one must continue to be ever vigilant in the fight to avoid field emitters.

The key to effective HPP processing is to force the peak fields during processing to the highest possible value. If this field is not raised, no benefits are observed. It was found that conditioning for longer times at the same field level, or with longer pulses at the same field level, did not help to reduce field emission significantly, or to reach higher fields. To obtain field emission *free* behavior at a certain operating field level it is necessary to condition cavities to even higher values — i.e., to approximately twice the operating field,

An important benefit of HPP is that it can be applied to recover cavities that may have been accidentally contaminated, e.g., in a vacuum mishap.

V CLOSING REMARKS

We have reviewed the evidence to show that field emitters are microparticles with the consequence that particulate cleanliness is essential to avoid field emission and

to reach high electric fields. The presence of a microparticle does not guarantee emission. Other conditions, such as the microgeometry of the particle, the nature of the adsorbates on the particle and the nature of the interface between the particle and the substrate play important roles.

We have discussed the chain of events from field emission to voltage breakdown. Field emission current heating leads to gas evolution from the surface and the melting of parts of the emitter. Ionization by the emission current leads to a charge build-up in the cloud of gas that hangs over emitter. With the high voltage between the ion-cloud and the surface, the emission current grows unstably. Eventually there is a spark between the cloud and the emitter, destroying the emitter and producing one or several craters. In RF cavities, such breakdown can be beneficial in rendering particulate emitters harmless by destroying the particles in the explosion. The goal is to reach high electric fields near the emitter so as to trigger the processing spark. Techniques that enhance the conditions for the formation of such a spark will improve the processability of RF cavities.

REFERENCES

1. C. M. Lyneis, in *Proceedings of the 1st Workshop on RF Superconductivity*, edited by M. Kuntze, page 119, KFK, Karlsruhe, Germany, 1980, KfK-3019.
2. R. J. Noer, Appl. Phys. A, Solids Surf. **28**, 1 (1982).
3. W. Weingarten, in *Proceedings of the 2nd Workshop on RF Superconductivity*, edited by H. Lengeler, page 551, CERN, Geneva, Switzerland, 1984, CERN.
4. G. Loew and J. W. Wang, in *Proceedings of the XIII International Symposium on Discharges and Electrical Insulation in Vacuum*, page 480, Paris, France, 1988, SLAC-PUB-4647.
5. H. Padamsee, in *Proceedings of the 4th Workshop on RF Superconductivity*, edited by Y. Kojima, page 207, KEK, Tsukuba, Japan, 1990, Rep. 89-21.
6. D. Moffat et al., Part. Accel. **40**, 85 (1992).
7. R. V. Latham, editor, *High Voltage Vacuum Insulation*, Academic Press, 1995.
8. G. A. Mesyats and D. I. Proskurovsky, *Pulsed Electrical Discharge in Vacuum*, Springer-Verlag, 1988.
9. R. H. Fowler and L. Nordheim, Proc. R. Soc. Lond. A, Math. Phys. Sci. **119**, 173 (1928).
10. P. Niedermann, PhD thesis, U. of Geneva, 1986, No. 2197.
11. C. Chianelli et al., In Sundelin [37], page 700.
12. B. Bonin, In Sundelin [37], page 1033.
13. J. Graber, PhD thesis, Cornell University, 1993.
14. J. Graber, Nucl. Instrum. Methods Phys. Res. A, Accel. Spectrom. Detect. Assoc. Equip. **350**, 582 (1994).
15. J. Knobloch, PhD thesis, Cornell University, 1997.
16. K. Saito et al., In Sundelin [37], page 1151.
17. N. Pupeter, in *Proceedings of the 7th Workshop on RF Superconductivity*, edited by B. Bonin, page 67, Gif-sur-Yvette, France, 1995, CEA/Saclay 96 080/1.

18. D. Kapner, Private communication, Internal Report.
19. M. Jimenez et al., J. Phys. D, Appl. Phys. **27**, 1038 (1994).
20. C. B. Duke and M. E. Alferieff, J. Chem. Phys. **46**, 923 (1967).
21. E. Mahner, In Sundelin [37], page 252.
22. R. V. Latham, Diagnostic studies of prebreakdown electron "pin-holes", In Latham [7], pages 61–113.
23. T. Hays et al., In Sundelin [37], page 750.
24. J. W. Wang and G. A. Loew, in *Proceedings of the 1989 IEEE Particle Accelerator Conference*, page 1137, 1989, IEEE Cat. 89CH2669-0.
25. J. Wynn and D. Kapner, Field emission studies of intentionally placed emitters in the mushroom cavity, SRF SRF980511-03, Laboratory of Nuclear Studies, Cornell University, 1998.
26. B. Jüttner, Physica **114C**, 255 (1982).
27. E. A. Litvinov et al., Sov. Phys.-Usp. **26(2)**, 138 (1983).
28. G. A. Mesyats, IEEE Trans. Electr. Insul. **18(3)**, 218 (1983).
29. B. Jüttner, IEEE Trans. Plasma Sci. **15(5)**, 474 (1987).
30. J. Knobloch et al., in *Proceedings of the 1995 Particle Accelerator Conference and International Conference on High Energy Accelerators*, page 1623, Dallas, TX, 1996, Cat. No. 95CH35843.
31. MASK, SAIC Corp., McLean, Va. 22102.
32. P. Bernard et al., in *Proceedings of the 1992 European Particle Accelerator Conference*, edited by E. H. Henke et al., page 1269, Editions Frontieres, 1992.
33. P. Kneisel et al., In Sundelin [37], page 628.
34. J. Graber, Nucl. Instrum. Methods Phys. Res. A, Accel. Spectrom. Detect. Assoc. Equip. **350**, 572 (1994).
35. C. Crawford et al., Part. Accel. **49**, 1 (1995).
36. W.-D. Möller and M. Pekeler, in *Proceedings of the 5th European Particle Accelerator Conference*, edited by S. Myers et al., page 2013, Barcelona, Spain, 1996, IOPP Publishing, Bristol.
37. R. M. Sundelin, editor, *Proceedings of the 6th Workshop on RF Superconductivity*, CEBAF, Newport News, Va., 1994.